

PAPER • OPEN ACCESS

Validation of theory-based models for the control of plasma currents in W7-X divertor plasmas

To cite this article: A. Dinklage *et al* 2021 *Nucl. Fusion* **61** 126022

View the [article online](#) for updates and enhancements.

You may also like

- [\(Expected difficulties with\) density-profile control in W7-X high-performance plasmas](#)
C D Beidler, Y Feng, J Geiger *et al.*
- [W7-X and the sawtooth instability: towards realistic simulations of current-driven magnetic reconnection](#)
Alessandro Zocco, Alexey Mishchenko, Carolin Nührenberg *et al.*
- [Isomon instabilities driven by energetic ions in Wendelstein 7-X](#)
Ya.I. Kolesnichenko, A. Könies, V.V. Lutsenko *et al.*



IOP | ebooks™

Bringing together innovative digital publishing with leading authors from the global scientific community.

Start exploring the collection—download the first chapter of every title for free.

Validation of theory-based models for the control of plasma currents in W7-X divertor plasmas

A. Dinklage^{1,*}, G. Fuchert¹, R.C. Wolf¹, A. Alonso², T. Andreeva¹, C.D. Beidler¹, M. de Baar³, Y. Gao¹, J. Geiger¹, M. Jakubowski¹, H. Laqua¹, N. Marushchenko¹, U. Neuner¹, N. Pablant⁴, A. Pavone¹, K. Rahbarnia¹, J. Schmitt⁵, H.M. Smith¹, T. Stange¹, Yu. Turkin¹ and the W7-X Team^a

¹ Max-Planck-Institut für Plasmaphysik, Greifswald, Germany

² CIEMAT, Madrid, Spain

³ DIFFER, Eindhoven, Netherlands

⁴ PPPL, Princeton, NJ, United States of America

⁵ Auburn University, Auburn, AL, United States of America

E-mail: dinklage@ipp.mpg.de

Received 24 June 2021, revised 15 September 2021

Accepted for publication 6 October 2021

Published 28 October 2021



CrossMark

Abstract


A theory-based model for the control of plasma currents for steady-state operation in W7-X is proposed and intended for model-based plasma control. The conceptual outline implies the strength of physics-based models: it offers approaches applicable to future conditions of fusion devices or next-step machines. The application at extrapolated settings is related to the validity range of the theory model. Therefore, the predictive power of theory-based control models could be larger than for data-driven approaches and limitations can be predicted from the validity range for the prediction of bootstrap currents in W7-X. The model predicts the L/R response when density or heating power is changed. The model is based on neoclassical bootstrap current calculations and validated for different discharge conditions. While the model was found to be broadly applicable for conducted electron-cyclotron-heated discharges in W7-X, limits were found for cases when the polarization of the electron cyclotron heating was changed from X2 to O2-heating. The validity assessment attempts to quantify the potential of the derived model for model-based control in the operational space (density, heating power) of W7-X.

Keywords: Wendelstein 7-X, bootstrap current, plasma control, stellarators, model validation, neoclassical modelling

(Some figures may appear in colour only in the online journal)

* Author to whom any correspondence should be addressed.

^a See Sunn Pedersen *et al* 2021 (<https://doi.org/10.1088/1741-4326/ac2cf5>) for the W7-X Team.

 Original content from this work may be used under the terms of the [Creative Commons Attribution 4.0 licence](https://creativecommons.org/licenses/by/4.0/). Any further distribution of this work must maintain attribution to the author(s) and the title of the work, journal citation and DOI.

1. Preparation for steady-state operation on Wendelstein 7-X: the need for robust control of long-pulse operation

Wendelstein 7-X (W7-X) is a superconducting fusion device built as a proof-of-principle to demonstrate the reactor potential of optimized stellarators [1]. To this end, plasma scenarios for high-power, long-pulse operation need to be developed. The plasma performance target is to provide conditions as close as achievable to fusion power plant conditions. In terms of dimensionless plasma parameters, the collisionality needs to be sufficiently small to examine stellarator-specific losses from the hot plasma centre. Therefore, the stellarator 3D-magnetic field requires an effective mitigation of neoclassical $1/\nu$ energy losses (with ν being the collision frequency), leading to a detrimental scaling of energy losses Q_{loss} with temperature T as high as $Q_{\text{loss}} \propto T^{4.5}$ [2]. W7-X mitigates these losses by minimizing transport from ripple trapped particles by shaping the magnetic field. W7-X is also seen as a first-of-a-kind *helical axis advanced stellarator* (HELIAS) [3] implementing the concept of stellarator optimization. The coil currents in W7-X are flexible to examine both the efficacy of optimized HELIAS fields (in the so-called standard and high-mirror configurations) but also to assess the effects of de-optimized magnetic field configurations. The optimization of the HELIAS magnetic field, moreover, includes aspects aside the reduction of transport from ripple-trapped particles such as MHD stability and reduced bootstrap current [3]. The reduction of neoclassical plasma losses has been experimentally demonstrated even in early operation phases of W7-X with fairly small heating power [4]. Relevant to the economic prospects of a fusion reactor concept, the optimization benefits further from the diamagnetic effect at high volume-averaged plasma beta values ($\beta = 4\%$) [5].

Consequently, the validation of the physics design of W7-X requires simultaneous attainment of high $\langle\beta\rangle$ and low collisionalities ν^* in equilibrated plasmas ($T_e \sim T_i$). In parallel, the leading operation target is to achieve pulses as long as 30 min, limited only by infrastructure constraints [6]. At present, in 2021, W7-X is being equipped with water-cooled plasma-facing components. Heating and fuelling upgrades are being installed along with extended wall surveillance and measures to detect high, localized power loads. The device is being upgraded with actively cooled plasma-facing components to sustain 10 MW-class heating power for up to 30 min. Ultimately, the forthcoming campaigns aim at a power throughput of 18 GW_s [7].

For the operation in forthcoming experimental campaigns, all actuator actions need to be integrated to arrive safely at the envisaged performance. To this end, appropriate plasma control schemes need to be qualified to ensure safe and reliable device operation. This motivation serves as a background for this prototypical study which is to put forward theory-based models for control. With the progress of 3D plasma theory, the development of predictive, theory-based tools for safe long-pulse operation comes more and more within reach for scenario preparation. To this end, this paper describes an

approach to develop theory-based models customized for control applications on W7-X. Differently to purely data-driven approaches, the main benefit of theory-based approaches is seen in its predictive power allowing one to expect a wide applicability when new parameter ranges are explored or for the assessment of scenarios in future devices. As a general concept, the use of theory-based models for tokamak control applications was reported in this conference [8]. A predictive scenario development employing a combined density and heating control to reduce the impact of bootstrap current in W7-X has been reported in [9]. The central novelty of this study is the validation of theory-based bootstrap current models with data-sets from W7-X experiments and the identification of limitations of the model in terms of the heating power and density. A key physics result in this paper is to explain the mechanism of bootstrap current reversal in the transition from attached to detached divertor plasmas.

The specific application of the model developed in this paper addresses the same issue as in reference [9]: in order to operate W7-X with an island divertor in long pulses at high-performance, the island divertor (see, e.g. [10, 11]) needs to handle high-power loads. The working principle of the island divertor employs strike-lines guiding particles and the non-radiated fraction of energy to the exhaust system [11]. The strike-lines appear due to the intersection of a large magnetic island emerging from an $\iota = 5/m$ ($m = 4, 5, 6$ are possibilities in W7-X) resonance of the rotational transform. The position of the island and thus the position of the strike-lines is sensitive to perturbations from plasma currents [12]. Despite being minimized and much smaller than in tokamaks [13] (at most a few 10 kA), the remnant neo-classical bootstrap current depends on heating power, density and settings of the magnetic field [14]. The effect of the pressure-driven bootstrap current is observed to shift the strike-lines [11] and thus its control is required. Electron-cyclotron-current drive is found to be a reliable actuator to impose compensating current [15]. Therefore, predicted plasma currents can be used to control the strike-line position by adjusting the current-drive from an electron-cyclotron current drive system. In W7-X, the current drive can be adjusted by front-steering mirrors [16]. While a fully predictive electron cyclotron current drive (ECCD) simulation from measured plasma profiles cannot be conducted sufficiently fast for immediate control applications, simplified models can provide control input within response times required to react on strike-line changes. To summarize the motivation behind this paper, strike-line control is expected to be key to achieve long-pulse operation, especially when higher heating power becomes available in future campaigns leading to higher bootstrap currents.

2. Theory-based models for control—a conceptual approach

Before the specific model development is discussed, the conceptual approach is described. Being explained in more detail in the course of this paper, the control-workflow elements will

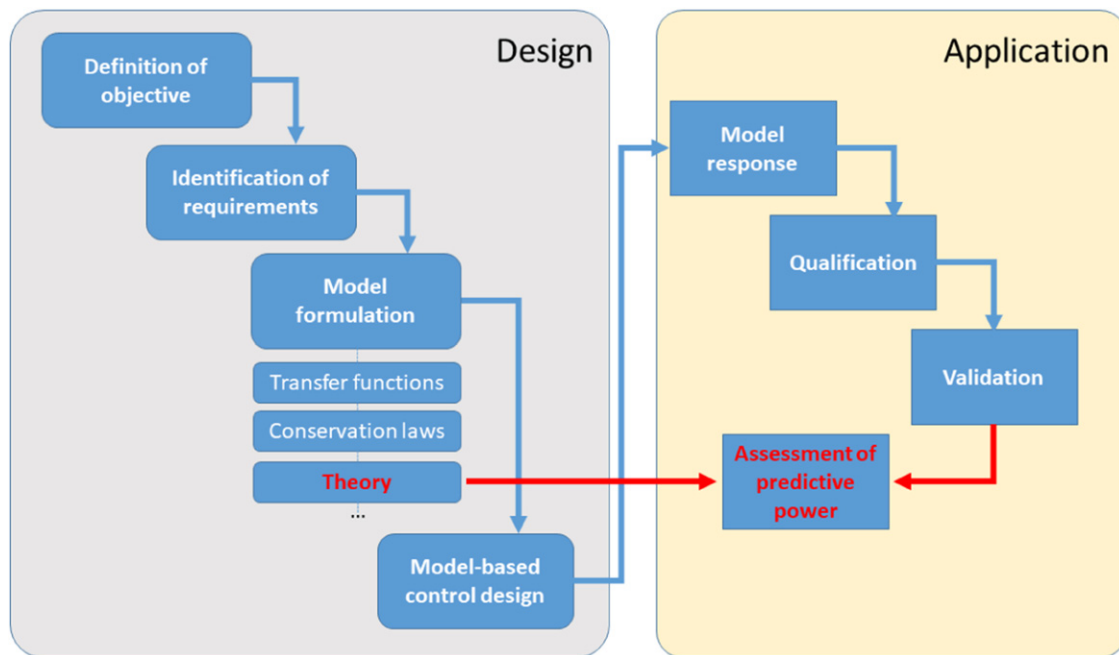


Figure 1. Workflow for the design and the qualification of model based design (adapted from [18]).

be specified in advance. Figure 1 shows the main elements for model-based control. An example for which the scheme has been applied is the RAPTOR framework [17]. The design and application domain is separated but understood to allow iterations not shown in figure 1. Usual steps involve the definition of the control objective (here the control of divertor strike-lines). The identification of requirements includes the required response times to avoid overloads and involves the specific properties of actuators and sensors.

Here, we focus on the model formulation and model validation steps (indicated in red). For the model formulation, different successful approaches have been applied such as transfer functions but also physics constraints. Here, we employ theory models for the formulation of the control model. As will be outlined below, a transport model applied on plasma profiles is reduced to a parametrized response function. This result can be exploited for a model-based control design. Although not addressed in this paper, it is of use to consider the application domain of the controller as outlined in figure 1. The deployment of the controller needs a qualification to assess the model response to sensors and actuators. At the end of the qualification process, an independent validation of the model could be made by measurements independent from the sensor signals used for the control design. The validation step should result in figures of a metric (e.g. the deviation from expected to measured plasma current) that allows one to quantify when the controller is expected to work.

The validation step opens the door to assess the control model in terms of predictive power. This may result in the benefit of transferring a control design developed at lower-performance devices to up-scaled machines or to adapt a physics-model-based controller for upgrades of a device. This

property appears to be fundamentally different than purely data-driven approaches, the validity of the latter is hardly expected to be predictable for unexplored plasma parameters. The expected applicability of theory-based models, however, is expressed by the validity of the underlying physics model: if the validity of the theory approach covers newly achievable plasma parameters, a theory-based controller appears to be the best-knowledge design for a controller that can be provided in advance. As a vision, theory-based control might find an application in predictive integrated discharge simulations. The IMAS framework of ITER [19] formally allows an integrated discharge plasma and control simulation (*flight-simulation*) and efforts on existing devices are underway [20].

The added value from the approach proposed in this paper emerges from the systematic use of theory derived from first principles. It is assumed that the use of theory implies a validity range of the physics-based model equivalent to the validity range of the underlying theory. Specifically, sensor data (from plasma diagnostics) are fitted and subsequently modelled with a neoclassical transport model to calculate key parameters describing the plasma response. A simplified physics model is the outcome of the model development described in this paper. The main benefit of the model-based approach is seen to avoid analysis and modelling steps that need too long processing times being incompatible with requirements of a plasma control system while still being sufficiently accurate to describe the observed plasma currents. And rather than implementing a full control application and qualification sequence (application domain in figure 1), this paper also focuses on the validation of the model to provide a first discussion on the potential for extrapolating the model to scaled parameters (i.e. the model's predictive power).

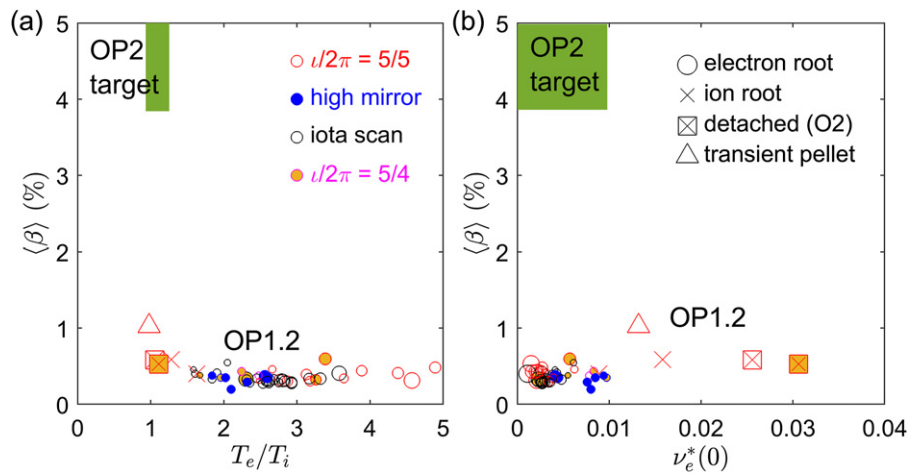


Figure 2. Operation space of W7-X test-divertor discharges (OP1). (a) and (b) show the electron to ion temperature ratio T_e/T_i and central electron collisionality $\nu_e^*(0)$, respectively, vs the volume averaged plasma beta $\langle\beta\rangle$. The colours show different magnetic configurations. The symbol reflects plasma states. O2 refers to electron cyclotron heated plasma in O2 polarization. Target values for the forthcoming campaigns OP2 (green patches) are shown for reference.

3. Definition of objectives: survey of achieved discharge characteristics in W7-X and future targets

In order to specify the control objectives in figures reflecting plasma properties, the expected plasma beta and collisionalities for reactor-like conditions for W7-X are shown in figure 2. The plots show a projection of the operation space from conducted campaigns in terms of plasma beta $\langle\beta\rangle$, core electron collisionalities $\nu_e^*(0)$ and T_e/T_i -ratio target parameters. The data result from a systematic transport modelling of W7-X discharges from recent campaigns with an uncooled divertor ('OP1': limited in pulse lengths $\tau_{\text{pulse}} < 100$ s) and heating power $P < 7$ MW). The modelled discharges encompass a density range from $n_e = (2 \dots 12) \times 10^{19}$ m. All plasmas shown in figure 2 were heated with electron cyclotron heating (ECH) in X2- or O2 polarization. Target values in figure 2 were chosen to be $\langle\beta\rangle > 4\%$ and $\nu_e^*(0) < 0.02$. At fusion conditions, it is the ion collisionality that is relevant. Thermal equilibration of electrons and ions ($T_e \sim T_i$), however, is expected at high densities for expected reactor scenarios.

The data in figure 2 indicate stable, stationary discharge conditions with one selected exception showing a transient high-performance pellet injection case (red triangle). For the subset of discharges heated by electron cyclotron heating (ECRH) with $T_e \gg T_i$, a clamping of the ion temperature typically occurs [21]. Moreover, most discharges have low plasma beta. Small collisionalities having target values indicated by the green regions, appear to be attainable given the achieved result. But many plasmas are found to be in a stellarator-specific transport regime that is not expected to occur under reactor conditions. These core electron-root confinement discharges (indicated by circles in figure 2) have large portions of the plasma affected by large positive radial electric fields E_r and regions of large shear of E_r within the plasma (see next section). These conditions, along with unfavourable ion-to electron temperature ratios are not expected for reactor

operation. As indicated in figure 2, electron-root conditions show up for even wider ranges when the magnetic configuration is altered to the high-iota divertor configuration ($\iota = 5/4$), or if a higher toroidal mirror is introduced (high-mirror data) or by scanning the rotational transform and in a scan from $\iota = 5/5 \rightarrow 5/4$ [22, 23]. On the other hand, steady-state compatible detached plasmas have been attained [7, 11, 24] already but are operating at fairly high collisionalities. And even the best plasma performance (red triangle in figure 2) in W7-X [25, 26] is far from the performance targets. The gap to reactor conditions did not come unexpectedly: W7-X is not yet equipped with the heating power to obtain the required increase of $\langle\beta\rangle$ at low ν^* and $T_e \approx T_i$ at high density. Heating upgrades are underway [7].

4. Model formulation and validation: a simplified model for the prediction of plasma currents in W7-X from neoclassical transport calculations

The L/R response model are solutions of the inhomogeneous differential equation for an LR circuit:

$$\frac{L}{R} \frac{dI(t)}{dt} + I(t) = I_{\text{cd}} + I_{\text{ref}} \quad (1)$$

with the inhomogeneous part $I_{\text{cd}} + I_{\text{ref}}$ chosen here to separate the current in the plasma at a reference time (the initial value of equation (1)) and a driven current I_{cd} . In cases current drive was applied (not considered in this paper), the offset I_{cd} could be calculated with current drive simulations. In case electron cyclotron current or neutral beam injection were applied, a ray tracing code for ECCD (TRAVIS [27]) and neutral beam current drive (BEAMS3D [28]), respectively, are in place to determine I_{cd} . For the neoclassical simulations conducted here, the plasma profiles and information on Z_{eff} was the required information for determining additional currents carried by the plasma. Again, this input is considered to be stationary shortly

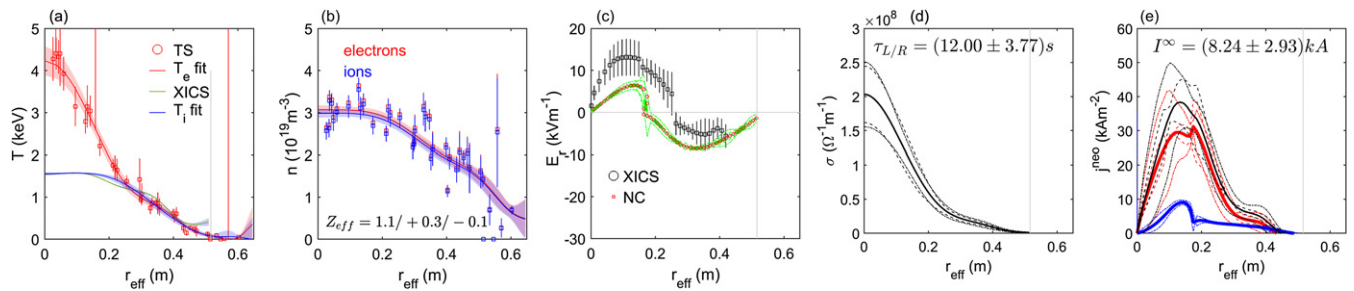


Figure 3. Profiles of W7-X discharge 20 180 927.033 for stationary conditions at $t = 3.5$ s (TS: Thomson scattering, XICS: x-ray imaging spectroscopy). (d) and (e) are results from modelling with the transport code NTSS employing transport coefficients calculated with the drift kinetic equation solver DKES. Red lines correspond to electrons, blue ones to ions and black lines refer to total values. The broken lines correspond to error estimates from fitting errors (dashed) and Z_{eff} uncertainties (dot-dashed).

after the heating power and the plasma density are set (i.e. typically within an energy confinement time) but lasting on the long L/R time scale.

The simplified physics model applied in this paper is the step-response of the plasma current set by the plasma resistance R and inductance L . The plasma acts to shield non-inductive currents: the bootstrap current arising due to the pressure gradients and to so-called current drive as a result of NBI or micro-wave heating. Consequently, the time response of the plasma current for a relaxation to stationary conditions (when plasma conditions are altered) is modelled by an ‘ L/R -response model’ reading as a response $I(t) = I^\infty [1 - \exp(-t/\tau_{L/R})]$ to a step-wise change of control parameters.

The key step for the derivation of quantitative, theory-based L/R -response models is calculating the stationary current I^∞ (which is a non-inductive current) and the response time $\tau_{L/R}$. The calculation of the neoclassical bootstrap current from plasma profiles is made by using the NTSS code [29]. The neoclassical modelling includes transport coefficients calculated from solving the drift-kinetic equation (DKES) [30] and includes effects from the radial electric field. The Ohmic resistance R is calculated with the parallel conductivity profile σ to be $R = R_0 / \int_0^a \sigma(r_{\text{eff}}) r_{\text{eff}} dr_{\text{eff}}$. The parallel conductivity and the bootstrap current are calculated from the DKES monoenergetic transport coefficient employing parallel momentum correction of the DKES solutions [31]. This approach ensures to capture deviations from the Spitzer conductivity due to trapped particles effective at low collisionalities. The calculation of the L/R time approximates L as the inductance of a conducting torus $L = R_0 \mu_0 (\ln(8R_0/a) - 2)$ with the plasma major radius R_0 , the minor radius a and the vacuum magnetic permeability μ_0 . W7-X has a large aspect ratio, so that $8R_0/a \sim 81$, and this approximation along with the neoclassical parallel conductivity can with good accuracy reproduce the current evolution in W7-X [14].

For the validation of the model conducted in this paper, experimental data are used (profiles of temperatures and densities) and stationary solutions of the transport model are calculated with NTSS. The time response is constructed from the stationary solution: the saturation level of the plasma current I^∞ is the bootstrap current I_{BS} . The response time is $\tau_{L/R}$. This construction implies its validity for periods the plasma profiles remain stationary.

The first example in figure 3 shows modelling for a typical discharge in OP1. The relevant result of the modelling is derived from the conductivity profile and the neoclassical bootstrap current density profile shown in figures 3(d) and (e). The stationary plasma current I^∞ is calculated to be the bootstrap current integrated up to the last closed flux surface (LCFS) $I^\infty = \int_{\text{LCFS}} j^{\text{neo}} dA$. External current drive was not considered here and was not expected from the settings of the electron cyclotron heating launch. To determine L/R , the plasma resistance was calculated from the conductivity profile in figure 3(d) and an estimate of the plasma inductance was obtained from an equivalent torus as described above.

These conductivity profiles $\sigma(r_{\text{eff}})$ and current density profiles $j_{e,i}^{\text{neo}}(r_{\text{eff}})$ (as functions of the effective minor radius r_{eff}) were ultimately obtained from measured plasma profiles as follows: for the electron temperatures and densities, data from a Thomson scattering (TS) system [32] are shown in figures 3(a) and (b). The ion temperature was measured with an x-ray imaging spectroscopy (XICS) system [33]. The ion densities were derived from the electron density data with a global correction for the effective charge Z_{eff} [34], assuming carbon (as the wall material) to be the main impurity. In order to process the data, fits were calculated employing Gaussian processes (with stationary Gaussian kernel and a fixed correlation length) [35]. The resulting error margins of the fit were used as the input for error estimate of the calculated currents and resistivity. The broken lines in figures 3(d) and (e) show simulation results from upper and lower bounds of the fits and Z_{eff} variations, respectively. The NTSS code processes the profile fits and calculates the ambipolar radial electric field shown in figure 3(c). As mentioned in the introduction, the shape of the radial electric field profile indicates a spatial bifurcation between solutions of the ambipolarity condition [36]: the large positive E_r is an indication for the so-called electron-root solution [37], whereas smaller negative radial electric fields indicate ion-root conditions. It is noted that the cross-over from electron- to ion-root comes with a large shear of the radial electric field typically showing up at around the largest electron temperature gradient or farther out. A comparison with measurements of the poloidal rotation by XICS indicated a good qualitative agreement [38]: the reversal of the field is found in XICS measurements and the magnitude of E_r is of the same order but not generally matching within error bands. The broader data set analysed in this paper indicates that the XICS

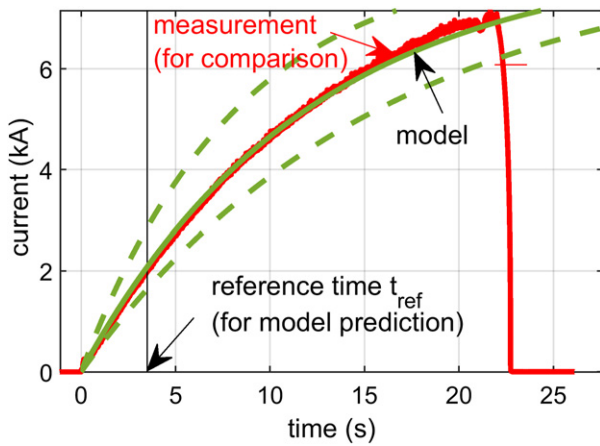


Figure 4. Measured plasma current and forward modelled bootstrap current from profile modelling at 3.5 s in the W7-X discharge 20 180 927.033. Dashed lines indicate expected model uncertainties.

cross-over lies further outside than the calculated one. The effect of the root transition is mainly seen in the ion bootstrap current density which is roughly halved at the transition point. The overall effect of E_r for the total current, however, is not exceeding uncertainties from the profile fitting or uncertainties from Z_{eff} .

Having conducted the calculation of the bootstrap current profiles and the plasma conductivity, the respective profiles are integrated to yield the parameters $\tau_{L/R}$ and I^∞ for the current-response model. In order to validate the results, the modelled current was compared to Rogowski coil measurements [39]. Figure 4 shows the L/R -response model with parameters derived from results shown in figures 3(d) and (e) at a reference time $t_{\text{ref}} = 3.5$ s early in the discharge. It is noted that good agreement (i.e. within the estimated uncertainty) of the model prediction is found when profile measurement in an early phase are used. The agreement of the measured plasma current and the modelled/predicted bootstrap current is almost perfect even for periods $t \gg t_{\text{ref}}$. It is therefore concluded that the plasma current evolution corresponds to the relaxation of the current initially shielding the bootstrap current. Moreover, it is concluded that the L/R -response model based on neoclassical bootstrap current calculations is validated for electron-root discharges. Limitations of the model are found in transient phases of plasma current redistribution, e.g. during plasma start-up or changes of the heating power and current drive with minor effects on the long-term current evolution. Limitations in terms of settings are discussed in the forthcoming section.

In view of the introduced operation targets of W7-X, transitions to divertor detachment are of particular interest. In the magnetic standard configuration, significant changes of the plasma current, even sign reversal, were observed when the plasma detached. In order to apply the model discussed above, the L/R -response model is modified to an initial value problem with changing boundary conditions when the plasma state is altered. While the simplified-model approach is not directly applicable, the modelled values for I^∞ and $\tau_{L/R}$ from experimental plasma profiles in attached and detached conditions can

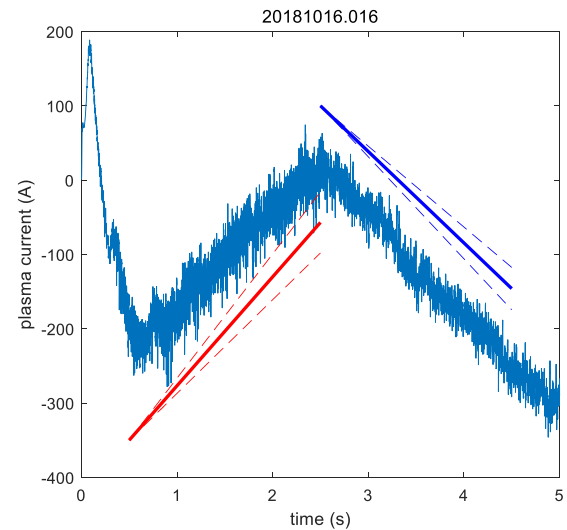


Figure 5. Plasma current evolution in a transition from attached to detached plasmas at $t = 2.5$ s. The lines indicate the modelled slope $I^\infty/\tau_{L/R}$. The slope of the current evolution is subject of the comparison and the initial value of the modelled slopes (solid lines; red: attached, blue: detached, broken lines for uncertainties) is shifted for convenience.

be determined and will be shown to explain the plasma current changes in the detachment transition.

As a second example, figure 5 shows a waveform of the plasma current indicating increasing plasma current in attached conditions and decreasing current for detached divertor plasmas. The detachment was induced by a gas puff at 2.5 s. The plasma profiles remain stationary for the attached and the detached phase, respectively except during plasma start-up ($t < 0.8$ s in figure 5). Having determined I^∞ and $\tau_{L/R}$ for each stationary period, the temporal change of the plasma current (and thus the change of the divertor strike-line) can be determined. For $t - t_0 \ll \tau_{L/R}$, the L/R response model can be approximated by $dI/dt \approx I^\infty/\tau_{L/R}$ reflecting a linear current response that can be calculated from the NTSS simulation results as outlined above. Figure 5 shows the calculated $I^\infty/\tau_{L/R}$ values for attached plasmas (red) to result in positive increasing values and the calculated $I^\infty/\tau_{L/R}$ (blue) values for detached plasmas to lead to a decrease of the plasma current with modelling errors of the corresponding slopes (broken lines). Figure 5 shows the slopes since the initial value of the current evolution I_{ref} in stationary phases is set by the plasma current attained in the start-up phase. The time response in this transient phase is not reflected by the simple model. But still the increase at stationary attached conditions and the decrease of the plasma current when the plasma is detached (and the resulting shift of the strike-lines) is found to be linear since the L/R time is much larger than the observation period. Therefore, the modelling refers to the change of the plasma current only. The blue and red lines shown in figure 5 show the modelled slopes shifted for convenience by an arbitrary off-set for two simulations. The red line indicates the change of the current calculated from stationary profiles in the attached phase (dashed lines show the error estimate of $I^\infty/\tau_{L/R}$) at 2.2 s. The blue line shows the $I^\infty/\tau_{L/R}$ in the detached phase with profiles

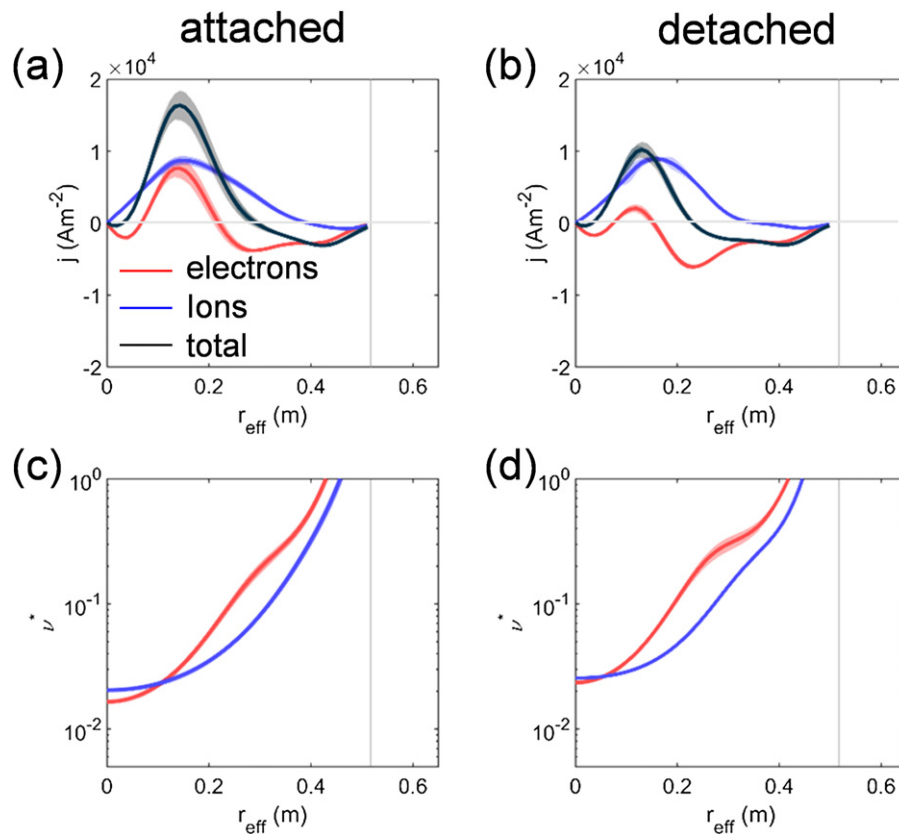


Figure 6. Stationary bootstrap current profiles [(a) and (b)] and collisionalities [(c) and (d)] for electrons and ions in discharge 20 181 016.016 calculated at $t = 2.2$ s (attached phase) and $t = 18.0$ s (detached phase).

taken at 4 s. In other words, the simple L/R -model based on neoclassical theory reasonably predicts the change in sign of the plasma current. This specific finding is of use to predict the reversed motion of the strike-lines on the divertor target when the plasma undergoes a transition to detachment. Having the bootstrap current modelling as a background, the change of the plasma current is understood to be a collisionality effect when then pressure profiles change in the transition to detachment.

To reveal the change in sign for dI/dt and we discuss the underlying mechanism of the current reversal. Figure 6 shows the bootstrap current profiles for the attached and detached phase of the standard magnetic configuration $\iota = 5/5$ discharge shown in figure 5. The ion bootstrap current profiles appears to be only barely affected by the change to detachment. In contrast, the electron bootstrap current profile changes significantly. In the plasma centre, the electron bootstrap current drops thereby decreasing the core electron contribution for the positive current direction. In between the core and the edge, the electron bootstrap current becomes negative in the detached phase. The total effect is a more negative electron bootstrap current profile in detached plasmas. The total bootstrap current profile is positively peaked close to the centre but negative for the plasma region outside about half of the minor plasma radius. Since the current profile is entering the total current weighted by r_{eff} to contribute more at larger minor radii, the stronger negative bootstrap current profile for $r_{\text{eff}}/a > 1/2$ in the detached phase (see figure 6) leads to the observed current reversal.

Thus, comparing figures 6(a) and (b) indicates the main difference of the plasma current in attached and detached phases to lie in the electron bootstrap current profile (red lines): the large electron bootstrap current peak at around $r_{\text{eff}} \approx 0.15$ m (figure 6(a)) is almost vanishing in detached plasmas (see figure 6(b)). The reason is seen in figures 6(c) and (d) which show a change in central electron collisionalities from attached to detached phases. In terms of temperatures and densities, the collisionality effect can be deduced from measurements: the ion temperature barely changes in the core in the transition from attached to detached plasmas. The change in the ion density (which is slightly peaking in the detached phase), leaves the collisionality profile of the ions virtually unaffected (blue lines in figures 6(c) and (d)). On the other hand, it is seen that the core collisionality of the electrons increases after detachment (red lines in figures 6(c) and (d)). Differently to the ions, the core electron response after detachment is a significant decrease of the electron temperature and with the slight density peaking, thus leading to the smaller core-collisionality of the electrons. The specific differences of ion and electron temperature profiles are due to the sources and sinks (ECRH for electrons in the very centre and some radiation in the plasma edge and collisional transfer for ion heating) and transport. While the neoclassical transport is calculated in the modelling, the remaining, substantial anomalous transport are subject of current research (see e.g. Ref. [40]).

In terms of the driving mechanism of the bootstrap current, it can be concluded that the effect of trapped electrons at low

collisionalities is becoming less pronounced in the plasma core of detached plasmas. This effect reduces the electron bootstrap current in the central plasma and causes the observed change in the plasma current. Summarizing the overall effect, it appears that the detachment leads to a pressure decrease at the LCFS and the reaction of the core plasma is a small density peaking and electron temperature decrease. While the whole set of interacting mechanisms is entangled but supported by experimental evidence from respective temperature and density mechanisms, an important conclusion can be drawn from the robustly observed current reversal shown in figure 5: the scrape-off layer plasma and the detachment mechanisms affect the plasma core. And the resulting current response leads to a change of the total current, thus the rotational transform and therefore on the strike line position.

5. Conclusions: discussing the validity of the theory-based model for plasma control

The examples discussed in the previous section show cases for which the neoclassical modelling and the simplified model match with the experimental findings. It is therefore concluded that the parallel transport assessed in this study is explained by neoclassical effects. It is noted, however, that the contribution of neoclassical mechanisms on perpendicular energy fluxes are different. Reports on the plasma confinement, even for plasmas at low electron collisionality, indicate a substantial difference between observed energy losses of the plasma energy and losses due to neoclassical transport [21, 25]. The difference of sinks and neoclassical energy flows with respect to sources is usually attributed to anomalous transport. The anomalous transport is usually assumed to result from plasma turbulence [40]. Since the underlying mechanisms of parallel and perpendicular transport are different, the agreement of observed plasma currents with neoclassical bootstrap current calculations is seen as a parallel neoclassical effect. Therefore, even plasmas dominated by anomalous energy transport can be expected to exhibit neoclassical plasma currents.

Now, the validity of the model in terms of the accessible parameter space is discussed. While the coil set of W7-X allows one to alter the magnetic configuration in terms of ripples and curvatures (see figure 2), we focus in this discussion on a single magnetic configuration compatible with divertor operation, (standard configuration $\iota = 5/5$). Since the heating power and the plasma density are the leading control parameters for the confinement, figure 7 shows a scatter plot indicating stable plasma conditions and one selected transient case at highest $nT_i^0\tau_E$ obtained in the first campaigns of W7-X.

The data of stable discharges are found to be limited in density for a given heating power as a result of a radiation density limit [41] depends on the wall conditioning and boronization had a beneficial effect on the accessible densities [42]. The circles indicate plasmas with core electron-root confinement. The size of the circle reflects the radial fraction of the plasma volume with positive radial electric field from modelling the ambipolarity condition. The case studied above is an electron-root discharge and lies around $3.5 \times 10^{19} \text{ m}^{-3}$ and 2 MW. While a number of co-settings, like wall conditions, are not the

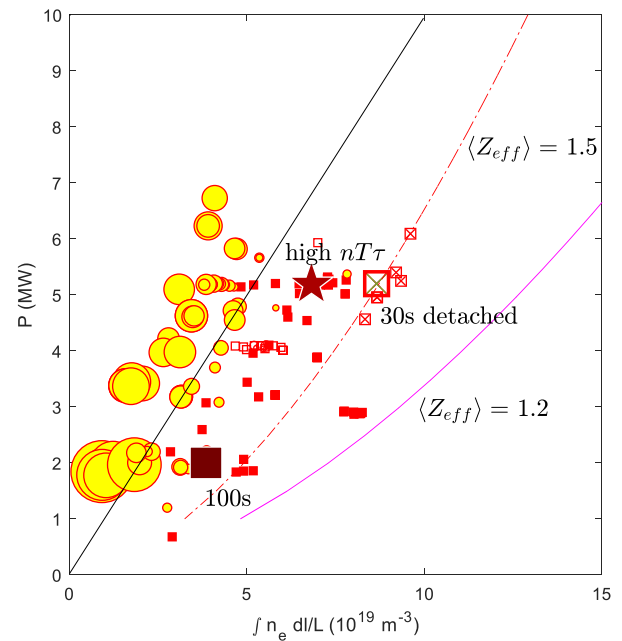


Figure 7. Operation space of electron cyclotron heated W7-X test-divertor-unit discharges (OP1) for the standard magnetic configuration. P is the heating power, the abscissa is the line averaged density. The magenta and broken red lines show density limits at different Z_{eff} . The black line corresponds to $P \text{ (MW)} = \bar{n} (10^{19} \text{ m}^{-3})$. Yellow symbols are electron-root discharges, red squares are ion-root discharges. Crossed squares correspond to detached cases.

same in the data set shown in figure 7 (see also [43]), some density scans indicate a super-critical transition to pure ion-root conditions with increasing density. As an experimental finding indicated by the black line in figure 7, electron-root conditions are found for $\bar{n} (10^{19} \text{ m}^{-3}) < P \text{ (MW)}$ in W7-X standard configuration discharges. Deviations of plasma currents from the model were found when magnetic islands are intentionally shifted inside the plasma [], differences are found both in I^∞ and $\tau_{L/R}$ (in the order of a few tens of percent). The difference due to magnetic islands (even beyond the flattening of the pressure profiles) is being investigated. General agreement for the L/R-model was found for electron-root discharges and adjacent ion-root discharges. For O2-heated, long-pulse discharges expected to be accessible in the forthcoming campaign OP2, systematic deviations in the predicted current occur. Differences may be due to ECCD from multi-pass reflections of strong microwave heating. These deviations can be addressed by inclusion of current drive calculations to determine I_{cd} in equation (1) for including current drive in the current response model.

While the specific use of the current-response model in a control application does not lie in the scope of this paper, the presented results allow one to discuss options for employing the simplified model. Typical L/R times in the order of some 10 s. The specific requirements on response times for the data analysis and the modelling are subject to detailed assessments for a respective controller implementation. Computing times in the order of some fractions of a second, however, do not appear to contradict with $\tau_{L/R}$. Codes to analyse profile data

are designed for a refined analysis without time restrictions and do not meet with the even roughly formulated requirements. An acceleration of (off-line) analysis codes is underway employing neural network techniques [44]. A complementary approach could take benefit from a high reproducibility of observed plasma profiles: a database linking control parameters (heating power, mean density, magnetic configuration) with profile shapes could be used to infer profile proxies with a smaller number of measurements that can be analysed more rapidly. As an example relevant to forthcoming campaigns of W7-X, the implementation of a multi-channel interferometer with fast FPGA based analyses [45] could be used for inferring density profiles. Likewise, a precomputation and parametrization of I^∞ and $\tau_{L/R}$ appears to be an option for a fast implementation of the modelling step to provide the required parameters for the physics based model for plasma control.










To conclude, the reported findings demonstrate the potential of theory-based, but reasonably simple time-response models to predict the plasma current in W7-X. The current reversal observed in detachment transitions is consistently modelled to be due to the electron response when the edge pressure is decreasing in detachment. Moreover, the validity of the model approach is discussed. The presented results can be applied for real-time control of changes in the edge rotational transform to have a direct effect on strike-line positions. An advantage of the simplified physics model is seen to be computationally much faster than full time-dependent modelling. The specific role of theory is to derive the model parameters. A parametrization in terms of control parameters and settings of the device is proposed to provide even a look-up proxy for the required model parameters. For a specific application, it is noted that electron-cyclotron current drive [46] could be used as an actuator and has been demonstrated to be fully in line with neoclassical calculations for the parallel transport. Further applications for the general approach of using physics models for control lie in the prediction of stored energy and density control. The validation of the approach on plasma data from W7-X is the background for the expectation that a physics-model-based control can be extrapolated to upgraded heating capabilities as expected in the next campaigns of W7-X. Ultimately, the model-based control approach contributes to the development of reliable plasma scenarios for next-step stellarators.

Acknowledgments

This work has been carried out within the framework of the EUROfusion Consortium and has received funding from the Euratom Research and Training Programme 2014–2018 and 2019–2020 under Grant Agreement No. 633053. The views and opinions expressed herein do not necessarily reflect those of the European Commission.

ORCID iDs

A. Dinklage  <https://orcid.org/0000-0002-5815-8463>
R.C. Wolf  <https://orcid.org/0000-0002-2606-5289>

A. Alonso  <https://orcid.org/0000-0001-6863-8578>
T. Andreeva  <https://orcid.org/0000-0003-2390-4240>
C.D. Beidler  <https://orcid.org/0000-0002-4395-239X>
Y. Gao  <https://orcid.org/0000-0001-8576-0970>
M. Jakubowski  <https://orcid.org/0000-0002-6557-3497>
N. Pablant  <https://orcid.org/0000-0001-6617-8459>
A. Pavone  <https://orcid.org/0000-0003-2398-966X>
K. Rahbarnia  <https://orcid.org/0000-0002-5550-1801>
J. Schmitt  <https://orcid.org/0000-0002-9407-7636>

References

- [1] Grieger G. et al 1992 *Phys. Fluids B* **4** 2081–91
- [2] Beidler C.D. et al 2011 *Nucl. Fusion* **51** 076001
- [3] Nührenberg J. and Zille R. 1986 *Phys. Lett. A* **114** 129–32
- [4] Beidler C.D. et al 2021 *Nature* **596** 221–6
- [5] Geiger J., Beidler C.D., Feng Y., Maaßberg H., Marushchenko N.B. and Turkin Y. 2015 *Plasma Phys. Control. Fusion* **57** 014004
- [6] Bosch H.-S. et al 2017 *Nucl. Fusion* **57** 116015
- [7] Sunn-Pedersen T. et al 2021 *Nucl. Fusion* (<https://doi.org/10.1088/1741-4326/ac2cf5>)
- [8] Staebler G. et al 2021 Advances in prediction of tokamak experiments with theory-based models *Nucl. Fusion* (submitted)
- [9] Sinha P., Böckenhoff D., Endler M., Geiger J., Hölbe H., Smith H.M., Pedersen T.S. and Turkin Y. 2019 *Nucl. Fusion* **59** 126012
- [10] Feng Y. et al 2021 *Nucl. Fusion* **61** 086012
- [11] Jakubowski M. et al 2021 *Nucl. Fusion* **61** 106003
- [12] Gao Y., Jakubowski M.W., Drewelow P., Pisano F., Puig Sitjes A., Niemann H., Ali A. and Cannas B. 2019 *Nucl. Fusion* **59** 066007
- [13] Dinklage A. et al 2018 *Nat. Phys.* **14** 855–60
- [14] Neuner U. et al 2021 *Nucl. Fusion* **61** 036024
- [15] Turkin Yu. et al (private communication)
- [16] Stange T. et al 2018 *EPJ Web Conf.* **157** 02008
- [17] Felici F., Citrin J., Teplukhina A.A., Redondo J., Bourdelle C., Imbeaux F. and Sauter O. 2018 *Nucl. Fusion* **58** 096006
- [18] de Baar M. 2021 (private communication)
- [19] Imbeaux F. et al 2015 *Nucl. Fusion* **55** 123006
- [20] Janky F., Fable E., Treutterer W., Gomez Ortiz I. and Kudlacek O. 2019 *Fusion Eng. Des.* **146** 1926–9
- [21] Beurskens M. et al 2021 Confinement in electron heated plasmas in Wendelstein 7-X and ASDEX Upgrade; the necessity to control turbulent transport *Nucl. Fusion* (submitted)
- [22] Geiger J. et al 2021 Confinement and equilibrium with internal islands in a configuration scan with respect to IOTA in W7-X 28th IAEA Fusion Energy Conf. (Nice, France, 10–15 May 2021) Paper EX/P6-4
- [23] Andreeva T. et al 2021 *Nucl. Fusion* (submitted)
- [24] Zhang D. et al 2019 *Phys. Rev. Lett.* **123** 025002
- [25] Baldzuhn J. et al 2020 *Plasma Phys. Control. Fusion* **62** 055012
- [26] Bozhnikov S.A. et al 2020 *Nucl. Fusion* **60** 066011
- [27] Marushchenko N.B., Turkin Y. and Maassberg H. 2014 *Comput. Phys. Commun.* **185** 165–76
- [28] Lazerson S.A. et al 2021 *Nucl. Fusion* **61** 096005
- [29] Turkin Y., Beidler C.D., Maaßberg H., Murakami S., Tribaldos V. and Wakasa A. 2011 *Phys. Plasmas* **18** 022505
- [30] Hirshman S.P., Shaing K.C., van Rij W.I., Beasley C.O. and Crume E.C. 1986 *Phys. Fluids* **29** 2951–9
- [31] Maaßberg H. et al 2009 *Phys. Plasmas* **16** 072504
- [32] Pasch E., Beurskens M.N.A., Bozhnikov S.A., Fuchert G., Knauer J. and Wolf R.C. 2016 *Rev. Sci. Instrum.* **87** 11E729

- [33] Pablant N.A. *et al* 2018 *Phys. Plasmas* **25** 022508
- [34] Pavone A. *et al* 2019 *J. Inst.* **14** C10003
- [35] Chilenski M.A., Greenwald M., Marzouk Y., Howard N.T., White A.E., Rice J.E. and Walk J.R. 2015 *Nucl. Fusion* **55** 023012
- [36] Maaßberg H. *et al* 1993 *Phys. Fluids B* **5** 3627
- [37] Yokoyama M. *et al* 2007 *Nucl. Fusion* **47** 1213–9
- [38] Pablant N. *et al* 2020 *Nucl. Fusion* **60** 036021
- [39] Rahbarnia K. *et al* 2018 *Nucl. Fusion* **58** 096010
- [40] Xanthopoulos P. *et al* 2020 *Phys. Rev. Lett.* **125** 075001
- [41] Fuchert G. *et al* 2020 *Nucl. Fusion* **60** 036020
- [42] Wauters T. *et al* 2018 *Nucl. Fusion* **58** 066013
- [43] Brezinsek S. *et al* 2021 Plasma-surface interaction in the stellarator W7-X: conclusion drawn from operation with graphite plasma-facing components *Nucl. Fusion* (submitted)
- [44] Pavone A., Svensson J., Langenberg A., Höfel U., Kwak S., Pablant N. and Wolf R.C. 2019 *Plasma Phys. Control. Fusion* **61** 075012
- [45] Brunner K.J. *et al* 2018 *J. Inst.* **13** P09002
- [46] Turkin Y., Maassberg H., Beidler C.D., Geiger J. and Marushchenko N.B. 2006 *Fusion Sci. Technol.* **50** 387–94